RESEARCH ARTICLE

Yessotoxin production and aerosolization during the unprecedented red tide of 2020 in southern California

Eva Ternon[1,2,*] ⓘ, Melissa L. Carter[3], Lucia Cancelada[4], Robert H. Lampe[3,5], Andrew E. Allen[3,5], Clarissa R. Anderson[6], Kimberly A. Prather[3,4], and William H. Gerwick[1,7]

An April–May 2020 bloom of the red tide microalga *Lingulodinium polyedra* developed to an unprecedented size, extending from northern Baja California to the Santa Barbara Channel. The *L. polyedra* strain is native to coastal California and is known to produce low levels of a toxic di-sulfated polyether named yessotoxin (YTX). In order to assess the evolution of the YTX content throughout the bloom and its transfer to water and aerosols, the concentration of YTX analogs was measured in the particulate and the dissolved organic matter of the sea surface water as well as in onshore sea spray aerosols. The YTX cell content was characteristic of Californian strains of *L. polyedra*. A lower production of YTX analogs by the cells at the peak of the bloom was detected, yielding total YTX content (particulate + dissolved) ranging from below the detection limit to 6.89 ng L^{-1} at that time. Yessotoxin and homo-yessotoxin were detected in sea spray aerosol measured onshore (from below detection limit to 20.67 $\pm$ 8.37 pg m^{-3}), constituting the first detection of YTX analogs in coastal aerosols. The aerosolized YTX did not correlate with the seawater content but rather with westerly winds and higher tides. The presence of YTX in aerosols motivates further investigation into potential correlations with adverse effects in humans.

Keywords: *Lingulodinium polyedra*, Yessotoxin, Sea spray aerosols, 18S rRNA genes, California

1. Introduction

Blooms caused by the dinoflagellate *Lingulodinium polyedra* are frequently observed in southern California. Commonly categorized by the descriptive term "red tide" due to discoloration of the water when blooming at high biomass (Dierssen et al., 2006), *L. polyedra* blooms are generally considered harmless to coastal populations, even though *L. polyedra* has the potential to produce yessotoxin (YTX; Armstrong and Kudela, 2006). YTX is a di-sulfated toxin also produced by the dinoflagellates *Protoceratium reticulatum* and *Gonyaulax spinifera* (Satake et al., 1997; Rhodes et al., 2006), with many structural analogs having been reported (Sala-Pérez et al., 2016). The levels of YTX produced by strains native to coastal Californian waters are very low (Armstrong and Kudela, 2006; Howard et al., 2008) in comparison to strains found in the Mediterranean Sea (Draisci et al., 1998; Paz et al., 2004). However, given the apparent global increase in harmful algal blooms (HABs), particularly dinoflagellate HABs (Hallegraeff, 2010; Hallegraeff et al., 2021) in response to environmental changes, the production of YTX associated with dinoflagellate blooms may pose an intensifying threat to coastal ecosystems and populations.

In 2020, a southern Californian "red tide" that extended from northern Baja California to the Santa Barbara Channel (Kahru et al., 2021) led to a widespread and unprecedented die-off event of fish and invertebrates (Skelton et al., n.d.). Although low dissolved oxygen levels (Wilson et al., 2022) are the most probable cause of mortality, high concentrations of YTX in the water column are a possible contributing factor to explain animal mortality (De Wit et al., 2014). In addition to the potential

[1] Center for Marine Biotechnology and Biomedicine, Scripps Institution of Oceanography, University of California San Diego, La Jolla, CA, USA

[2] Laboratoire d'Océanographie de Villefranche sur mer (UMR 7093), Sorbonne Université, CNRS, Villefranche-sur-mer, France

[3] Scripps Institution of Oceanography, University of California San Diego, La Jolla, CA, USA

[4] Department of Chemistry and Biochemistry, University of California San Diego, La Jolla, CA, USA

[5] Microbial and Environmental Genomics, J. Craig Venter Institute, La Jolla, CA, USA

[6] Southern California Coastal Ocean Observing System, Scripps Institution of Oceanography, University of California San Diego, La Jolla, CA, USA

[7] Skaggs School of Pharmacy and Pharmaceutical Sciences, University of California San Diego, La Jolla, CA, USA

*Corresponding author:
Email: eva.ternon@imev-mer.fr

production of particulate and dissolved toxins in the water column and transfer to the food web, some biotoxins produced by dinoflagellates are known to be aerosolized (Backer et al., 2005; Ciminiello et al., 2014; Medina-Pérez et al., 2021; Van Acker et al., 2021), such as the well-documented release of the neurotoxin brevetoxin into the atmosphere by Floridian blooms of *Karenia brevis* (Kirkpatrick et al., 2010).

Sea spray aerosols (SSA) are produced when air bubbles burst at the ocean surface (Lewis and Schwartz, 2004). They are known to contain a mixture of sea salt, biogenic particles (bacteria, viruses; Ault et al., 2013), as well as organic molecules such as carbohydrates, proteins (enzymes), and lipids (Patterson et al., 2016; Rastelli et al., 2017; Malfatti et al., 2019). The presence of YTX in SSA during a Californian dinoflagellate bloom has not been reported previously. Yet, a study of controlled cultures of another YTX-producer (*Protoceratium reticulatum*) in a marine aerosol reference tank demonstrated the transfer of one YTX analog, homoYTX, from the particulate and dissolved organic matter in seawater to the air in SSA (Van Acker et al., 2021). Although Alfonso et al. (2016) qualified YTX as a "different toxin" due to its mild toxicological effects, recent evidence of cell viability reduction by low concentrations of YTX was obtained using pulmonary cell lines (Van Acker et al., 2020); in theory, YTX could cause respiratory symptoms. To evaluate this potential from an environmental perspective, we investigated the production of YTX by wild *Lingulodinium polyedra* cells and its transfer to seawater and aerosols during the 2020 bloom period, using targeted analyses by liquid chromatography coupled to high-resolution mass spectrometry (LC-HRMS). The temporal evolution of the eukaryotic communities throughout the peak of the bloom was assessed through 18S rRNA gene sequencing.

2. Methods

The two following sampling strategies were conducted from Ellen Browning Scripps Pier in La Jolla, CA (32.8663°N, 117.2546°W), and combined to characterize the event: (i) high-frequency sampling constrained by the stay-at-home order during the COVID pandemic and performed at the peak of the bloom, daily between the April 23 and April 30, 2020, and every other day from April 30 to May 6; and (ii) long-term sampling, bi-weekly at a minimum, from March to June 2020 as part of an ongoing monitoring program for the Southern California Coastal Ocean Observing System, California Harmful Algal Bloom Monitoring and Alert Program (SCCOOS, CalHABMAP; Monday samples), and the McGowan Plankton and Chlorophyll Program at Scripps Institution of Oceanography (Thursday samples).

2.1. Sampling and cell counts

High-frequency sampling involved daily seawater collection around noon from the Scripps Pier at approximately 0.2 m depth using a 10 L bucket. Sampling was performed in triplicate (i.e., three buckets) except for the dissolved toxin content, which was sampled in duplicate. A 2 mL aliquot was fixed in Lugol's solution immediately after sampling and stored at 4°C until cells could be loaded on a Sedgewick-Rafter slide and counted via light microscopy (McAlice, 1971).

Long-term sampling consisted of surface seawater collection at approximately 0.5 m depth using an acid-washed 10 L bucket as described in Hatch et al. (2013). Samples were fixed with 4% formaldehyde and stored in the dark at room temperature until counting by first settling into Utermöhl settling chambers (no chamber, 10, or 50 mL), then counted at a range of volumes (0.48 mL to 2.50 mL) determined by cell density (Hasle, 1978).

2.1.1. Particulate and dissolved toxins

High-frequency sampling methods consisted of filtering 1 L through 47 mm GF/F filters (Whatman) and sub-filtering through 47 mm 0.2 μm filters (Supor® 200, Pall Corporation) using a peristaltic pump to avoid damaging the phytoplankton cells. Filtrate was collected in acid-washed PPE bottles, immediately placed in a cooler in the dark and then at −20°C within 1 h. GF/F filters were folded using clean tweezers, placed in an 11 mL glass vial containing 1.5 mL of methanol (MeOH, HPLC grade, Merck), and immediately vortexed for 1 min to ensure full extraction of the cellular content. Both the GF/F filters with MeOH and the filtrate were stored at −20°C until further treatment.

Long-term sampling for particulate toxins consisted of filtering 100 to 500 mL onto 25 mm GF/F filters as feasible without clogging. Filters were collected in duplicates and stored at −80°C in 2 mL microtubes within 1 h of collection. All filters were extracted three times with 5 mL of MeOH, followed by sonication for 10 min and centrifugation at 3000 rpm at room temperature. The three supernatants were collected and combined and further evaporated to dryness.

2.1.2. Aerosolized toxins

Aerosols were sampled opportunistically from April 24 to April 30, 2020, on the shore end of the Scripps Pier, at 10 m above sea surface. Aerosol sampling was curtailed due to widespread COVID-19 restrictions and stay-at-home orders. During typical onshore winds, the aerosol sampling site was downwind of the surf zone, an important source of SSA (van Eijk et al., 2011). Aerosols (total suspended particles) were collected onto combusted 47 mm quartz fiber filters (2500 QAT-UP, Pall Corporation) in two stainless steel filter holders (2220, Pall Corporation) hanging on the northern side of the pier for 24 h (noon to noon) at a pumping rate (air passed through the filters) of 40 m³ h⁻¹. To minimize contamination, filters were combusted at 500°C for 2 h prior to sampling and stored in combusted aluminum foil before deployment and after recovery. Laboratory blanks were combusted filters.

2.1.3. DNA

To monitor the eukaryotic microbial community structure, DNA samples were collected four times from April 22 to May 11, 2020, as part of the long-term sampling strategy (April 22, April 27, May 4, and May 11). Approximately 300–600 mL of seawater was filtered through a 0.22 μm

Sterivex-GP filter unit (Cat. no. SVGP01050, Millipore) that was immediately sealed with luer-lock plug and Hemato-Seal™ tube sealant, wrapped in aluminum foil, and flash-frozen in liquid nitrogen. The samples were stored at −80°C until extraction.

2.2. Toxin extraction and analysis
2.2.1. Particulate toxins
The vials containing the GF/F filters were centrifuged at 3000 rpm for 15 min. Preliminary analysis of raw cell extracts did not allow detection of YTX. Therefore, following the procedure developed by Ciminiello et al. (2003), the YTX were pre-concentrated, using 1.3 mL of the supernatant for the high-frequency samples and solubilizing the dry extract of the long-term samples. The residual extract was re-solubilized in 1 mL of 20 mM ammonium formate buffer (pH 5.8):MeOH (7:3, v/v), and the solution was loaded on a C18 solid phase extraction (SPE) column (200 mg, 3 mL, BondElut Agilent) activated with MeOH and equilibrated with the same buffer. The C18 column was washed with two column volumes of MeOH:water (3:7, v/v), and YTX and its analogs were eluted with two column volumes of isopropanol:water (2:8, v/v). The eluate was evaporated and the residue re-solubilized in 150 µL of MeOH and stored at −20°C until analysis. Triplicate blank GF/F filters were processed similarly.

2.2.2. Dissolved toxins
The seawater filtrates were extracted using PPL SPE cartridges (200 mg, 3 mL, BondElut, Agilent) following the recommendations by Dittmar et al. (2008), although at unmodified pH. The cartridges were activated with 3 mL of MeOH and equilibrated with 3 mL of MilliQ water. The seawater samples were then loaded on the cartridge, drop by drop, and the cartridge was subsequently rinsed with two column volumes of MilliQ water. Samples were eluted with two column volumes (6 mL) of MeOH and dried to a volume of 130 µL using a gentle stream of N_2. Triplicate blank samples consisted of 1 L of MilliQ water extracted following the same procedure. All samples were stored at −20°C until analysis.

2.2.3. Aerosolized toxins
Aerosol filters were cut into pieces and transferred to 50 mL Falcon tubes. They were extracted with 7 mL of MeOH while being sonicated for 10 min. The Falcon tubes were further centrifuged at 3000 rpm for 10 min, and the supernatant was transferred to a glass vial. The procedure was repeated three times, and the three extracts were combined and dried down to 150 µL using a rotavapor followed by a gentle stream of N_2. Three blank filters were also processed using a similar procedure. All samples were stored at −20°C until analysis.

2.2.4. UHPLC–HRMS analysis
The chemical content of the different samples was analyzed by ultra-high performance liquid chromatography coupled to high-resolution mass spectrometry (UHPLC-HRMS), using a Thermo Scientific Vanquish system (Thermo Scientific, USA). Separation was achieved on a UPLC C18 column (Kinetex® 2.6 µm, Polar C18, 150 × 2.1 mm, Phenomenex) maintained at 40°C. Eluent A was MilliQ water and Eluent B was a 95% acetonitrile:MilliQ water, with both eluents containing 50 mM formic acid and 3.5 mM ammonium formate. A gradient elution of 20% to 95% of B over 10 min was required for a combined analysis of YTX and its analogs. The flow rate was 500 µL min^{-1}, and the injection volume was 10 µL. Mass spectral data were acquired using an Orbitrap Elite MS mass spectrometer (Thermo Scientific, USA) equipped with an electrospray ionization source in the negative mode. Full scan spectra were acquired in the range of 200–2000 Da in the CID mode with a FTMS Analyzer set at a resolution of 120,000. Collision energies (CE) of 40 eV were applied to obtain the MS/MS spectra. The capillary voltage of the MS spectrometer was set at 3500 V, and the nebulizing parameters were set as follows: nebulizing gas (N_2) pressure at 0.5 bar, drying gas (N_2) flow at 11 L min^{-1}, drying temperature at 300°C, and the vaporizer/sheath gas temperature at 300°C.

A calibration curve was performed with a commercial mixture of toxins of the YTX-group purchased from Cifga®: >98.5% of YTX, <0.05% of 32-arabinoside YTX, <0.1% of 44,45-dihydroxy-41a-homoYTX, <0.1% of 9-Me-4-a homoYTX, 0.2% of 45-hydroxy-YTX, and 1.3% of nor-ring-A-YTX. Despite the absence of any reference for the homo-YTX (h-YTX), an ion at m/z (mass divided by charge number) 1155.4823 co-eluting with the YTX was tagged as the h-YTX and was quantified using the YTX as a reference. Extracted ion chromatograms (XIC) were obtained selecting the ion [M-H]$^-$ at m/z 1141.47 for YTX and m/z 1155.4823 for h-YTX, having matching retention time with the standard. The standard was diluted sequentially to obtain concentrations ranging from 0.30 ng mL^{-1} to 12 ng mL^{-1} of YTX. The detection limit of the instrument was 0.1 ng mL^{-1}, which can be propagated to 0.055 fg cell^{-1}. The sum of the YTX and h-YTX concentrations is described as total YTX hereinafter.

The analysis of the copepodamide content in the dissolved samples was based on the methods developed by Selander et al. (2015; 2019). The following m/z (precursor → diagnostic fragment) were targeted in the full scan LC-HRMS traces acquired in the negative mode: 760.5199 → 432.2798; 708.4886 → 432.2796; 732.4890 → 430.2641; 734.5045 → 432.2797; 758.5062 → 430.2650; and 706.4732 → 430.2641.

2.3. DNA extraction and 18S amplicon sequencing
DNA was extracted with the Macherey-Nagel NucleoMag Plant Kit for DNA purification (Cat. No 744400) on an Eppendorf epMotion 5057TMX, as described by Rabines et al. (2020). DNA was then assessed on a 1.8% agarose gel. Amplicon libraries targeting the V4 region of the 18S gene were generated via a one-step PCR using the Azura TruFi DNA Polymerase PCR kit with the V4F (CCAGCAS-CYGCGGTAATTCC) and V4RB (ACTTTCGTTCTTGATYR) primer set (Balzano et al., 2015). Each reaction was performed with an initial denaturing step at 95°C for 1 min followed by 30 cycles of 95°C for 15 s, 56°C for 15 s, and 72°C for 30 s. A volume of 2.5 µL of each PCR reaction was

run on a 1.8% agarose gel to confirm amplification. PCR products were purified using Beckman Coulter AMPure XP following the standard 1× PCR clean-up protocol. PCR quantification was performed using Invitrogen Quant-iT PicoGreen dsDNA Assay kit. Samples were then pooled in equal proportions followed by a 0.8× AMPure XP PCR purification. The final pool was then evaluated on an Agilent 2200 TapeStation and quantified with Qubit HS dsDNA kit. Sequencing was performed at the University of California, Davis Sequencing Core on an Illumina MiSeq (2 × 300 bp) with a 15% PhiX spike-in.

Amplicons were analyzed with QIIME2 v2020.06 (Bolyen et al., 2019). Briefly, demultiplexed paired-end reads were trimmed to remove adapter and primer sequences with cutadapt (Martin, 2011). Trimmed reads were then denoised with DADA2 to produce amplicon sequence variants (ASVs; Callahan et al., 2016). Taxonomic annotation of ASVs was conducted with the q2-feature-classifier classify-sklearn naïve-bayes classifier (Bokulich et al., 2018) against the full SILVA database (Release 138) that was curated with RESCRIPt (Robeson et al., 2021). The complete QIIME2 workflow is available on github (Allenlab, 2021).

3. Results

3.1. Eukaryote distribution

Cell abundance estimates for phytoplankton and ciliates, determined microscopically, were measured before, during, and after the bloom of *Lingulodinium polyedra*; percentage contributions were calculated from these cell counts (**Figure 1**). Diatoms were the dominant group before and after the bloom of *L. polyedra.* During the peak of the bloom, *L. polyedra* comprised 86%–99% of the plankton community. Cell abundances were over 1×10^6 cells L^{-1} for nearly 3 weeks, with the highest

recorded concentration of *L. polyedra* at 2.93×10^7 cells L^{-1} on April 30, 2020. This cell concentration is the highest for any phytoplankton species ever recorded throughout the 47-year Scripps Pier plankton observing history (1918–1927, 1930–1939, collected by EW Allen; 1992–2000, collected by J McGowan and colleagues; 2003–2007, collected by L Busse and colleagues; 2008–2020, collected by SCCOOS; NOAA ERDDAP, 2023). Another YTX producer, *Gonyaulax spinifera,* was observed at low abundances throughout the bloom, with peak cell count values observed on April 27 and April 30, 2020, at 5.22×10^4 and 9.51×10^4 cells L^{-1}, respectively. On April 30, many burst cells of *L. polyedra* were observed by microscopy (18%), followed by a new generation of cells on May 2. Starting on May 7, a rapid decline of *L. polyedra* was observed (**Figure 1**), while other unidentified dinoflagellates <20 μm increased along with several potential predators of *L. polyedra* (*Polykrikos* spp., *Noctiluca scintillans*, ciliates). In particular, ciliates were observed actively feeding on *L. polyedra* cells. A high number of lysed cells (8.6%) was observed again on May 14. This trend was confirmed by the molecular analysis (**Figure 2A** and **B**), which showed on May 11 a decrease to 21.2% of the relative abundance of *L. polyedra* among dinoflagellates, with a simultaneous emergence of other dinoflagellates species, such as members of the *Neoceratium* genus (12.7% of the total abundance of dinoflagellates). The molecular data also revealed a higher relative abundance of the three dinoflagellate predators *Polykrikos* spp., *Noctiluca* spp., and *Fragilidium* spp. compared to zooplankton predators towards the end of the bloom (**Figure 2A**). The most abundant copepod species prior to the bloom belonged to the Cyclopoida order; they were replaced by species of the Calanoida order towards the end of the bloom. The increasing relative abundance of Calanoida
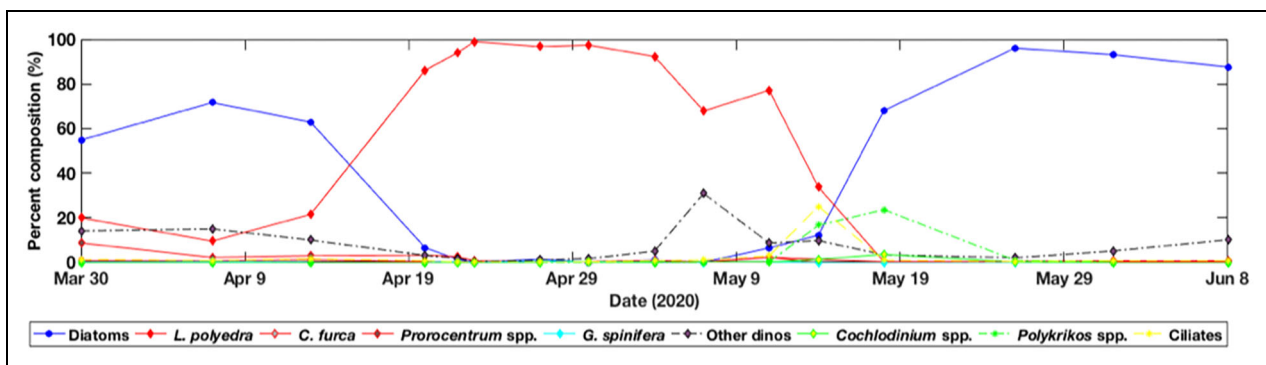

Figure 1. Microalgal diversity by percentage contribution during the course of the 2020 red tide. Percentage composition of eukaryotes determined from cell counts (by microscopy) from the start of the bloom to its end, March 30 to June 8, 2020. Phytoplankton were grouped to show relevant species: diatoms (blue lines), corresponding to the numeric sum across all observed species; bloom-forming species (red lines) *Lingulodinium polyedra, Ceratium furca, and Prorocentrum* spp.; slime-producing species (green lines) *Cochlodinium* spp.; and potential predators (dashed lines) *Gonyaulax spinifera* and other dinoflagellates, *Polykrikos* spp., and ciliates. The *L. polyedra* bloom started in early April, replacing a diatom bloom, before ending in mid-May, followed by a diatom bloom. Potential predators of *L. polyedra* were detected in early May with a peak in their percentage contribution coinciding with the bloom demise. Ciliates at the bloom demise were members of the Tintinnida order, mainly *Amphorellopsis acuta* and *Schmidingerella* spp.
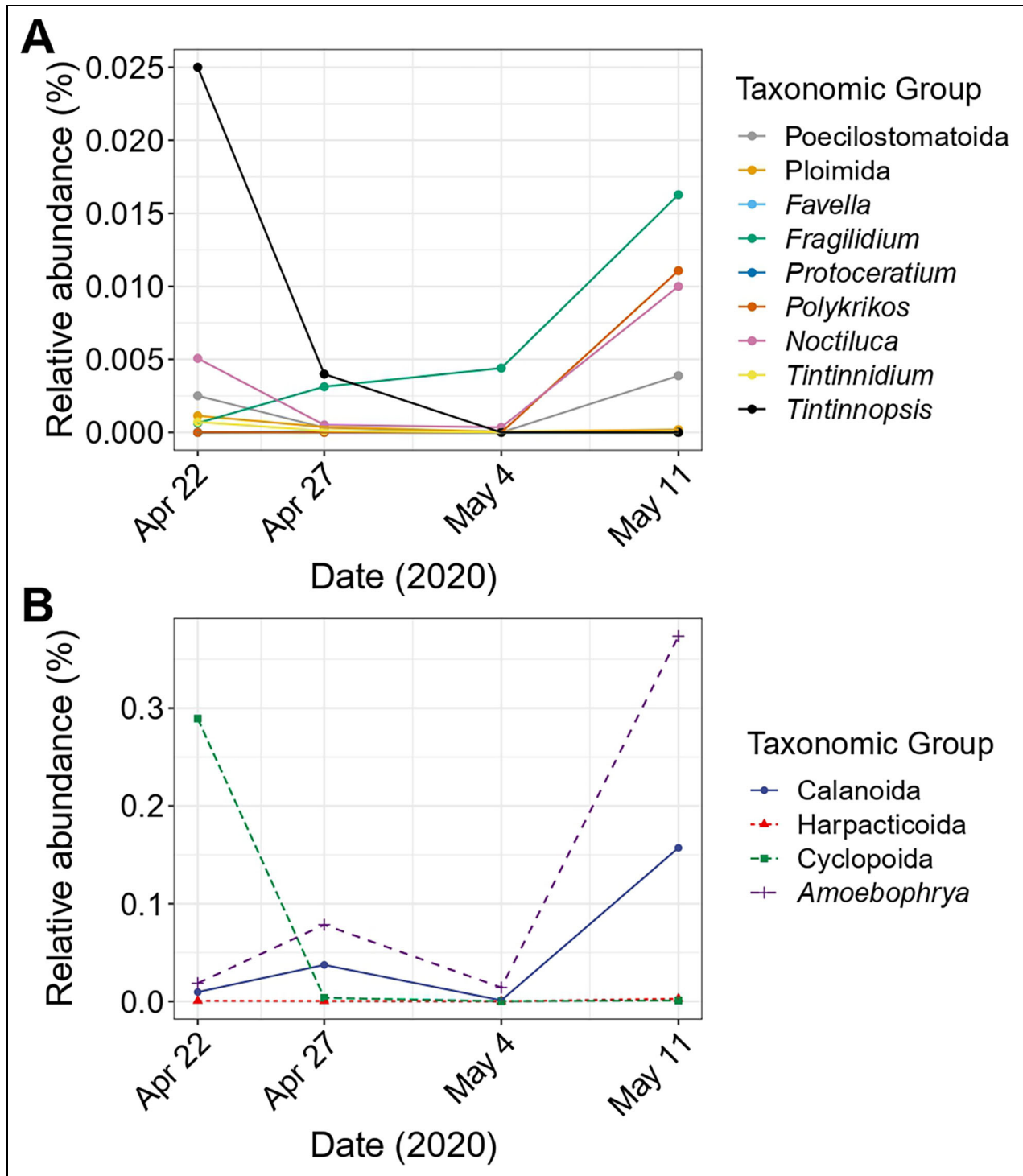
Figure 2. Diversity of potential predators of *Lingulodinium polyedra* by relative abundance during the 2020 red tide. Relative abundance (%) from all 18S-V4 amplicon sequences for the (A) potential predators of *L. polyedra* at the genus level and (B) arthropod orders and the *Amoebophyra* that were detected during the bloom. A compilation of all other taxonomic groups had a relative abundance of <0.2% (not depicted). The relative abundance of the potential predators of *L. polyedra* decreased as the bloom began and increased at bloom demise, when *Fragilidium* spp., *Polykrikos* spp., and *Noctiluca* spp. were particularly represented. Members of the Cyclopoida order present before the bloom were replaced by species of the Calanoida order after the bloom. The bloom demise was also accompanied by a sharp increase in species of the *Amoebophrya*.

was accompanied by a sharp increase of the relative abundance of the *Amoebophyra* genus (**Figure 2B**) to a higher extent than copepods (>0.3%). The bloom ended at this location around May 18, when *L. polyedra* dropped to less than 25% of the total phytoplankton community, while diatoms increased to above 68% (**Figure 1**).
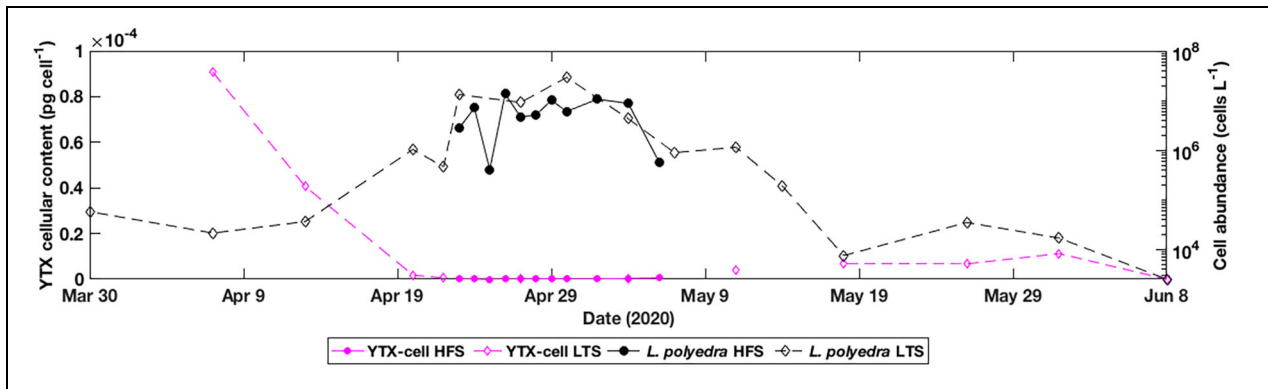
Figure 3. Yessotoxin content in *Lingulodinium polyedra* cells during the 2020 red tide. Comparison of the total yessotoxin (YTX) cellular content (pink dots, pg cell^{-1}) with the abundance of *L. polyedra* cells (grey dots, cells L^{-1}) through the course of the bloom. Long-term sampling (LTS) and high frequency sampling (HFS) are plotted with discontinuous line and continuous line, respectively. A lower toxin content was detected in *L. polyedra* cells during the peak of the bloom.

3.2. Cell concentration and cellular YTX production

Initially, the spatial distribution of the bloom was partially heterogeneous, with sampling inside or outside the dense bands of cells greatly influencing the total cell abundance (**Figure 3**) and contributing to the variability between replicates, including for the detection of YTX. Among known toxins of the YTX group, only the YTX and the h-YTX were detected in *Lingulodinium polyedra* cells. The proportion of h-YTX represented 15.8%–58.0% of the total YTX content, with a mean at 39.5% (Table S1) and no trend observed.

Two additional ions were observed by LC-MS^2 in the negative ion mode. These eluted 2 min after the reference YTX from Cifga® and showed values at m/z 1141.6318 and m/z 1155.6101, very close to the YTX (m/z 1141.4692) and h-YTX (m/z 1155.4823). These two unidentified ions yielded fragments at m/z 1061.6711 and m/z 1075.6714 (Figure S1), respectively, that are also close to YTX and h-YTX diagnostic fragments. While the identities of these fragments remain unknown, they are likely related to members of the YTX family.

The total YTX cellular content (reference YTX + h-YTX; the unknown metabolites above were not included in the calculation) was analyzed over the course of the bloom (particulate fraction, **Figure 3**), and ranged between the detection limit and 90.7 fg cell^{-1}. The maximal toxin content in cells was not measured at the peak of the bloom but rather during bloom initiation (April 7–14) and termination (May 26–June 1). When cell concentration was highest (April 20–May 4), the total YTX content was very low, ranging from the detection limit to 1.60 fg cell^{-1}.

3.3. Total yessotoxin content

The total particulate YTX concentrations were measured daily throughout the bloom between April 23 and May 6, 2020, and once a week otherwise (**Figure 4**). The particulate YTX concentrations varied significantly throughout the bloom. The highest values were measured not only at the peak of the bloom but also during bloom initiation and demise, consistent with the pattern of cellular YTX production. At the peak of the bloom, the total particulate YTX concentration was stable and ranged from detection limit to 3.36 ng L^{-1} (May 4). This low total YTX content was attributed only to *Lingulodinium polyedra* as it did not coincide with a significant increase in the abundance of *Gonyaulax spinifera*, another dinoflagellate known to produce YTX (**Figure 4A**).

Dissolved total YTX concentration (**Figure 4A**) was also measured opportunistically at the peak of the bloom (April 24 to May 6, 2020). The concentrations were similar, or even higher in some cases, to particulate YTX, ranging from 0.67 and 3.54 ng L^{-1}. The dissolved total YTX concentration increased throughout the bloom, reaching its maximum on May 4 after a short but dramatic decrease on April 30. The h-YTX represented 54.0% ± 4.12% of the total dissolved YTX content (Table S1), indicating a roughly equal distribution between dissolved YTX and h-YTX in seawater.

During April 24–30, 2020, samples for aerosolized total YTX were also collected (**Figure 4B**). Yessotoxin and h-YTX were detected in the collected aerosols on most sampling days, and their concentrations remained stable, with values ranging from the detection limit to 1.13 pg m^{-3} (YTX) and 1.42 pg m^{-3} (h-YTX), except on April 30, when concentrations suddenly increased to 13.0 ± 5.47 pg m^{-3} (YTX) and 7.65 ± 2.89 pg m^{-3} (h-YTX). On April 30, the total YTX concentration in the aerosols reached 20.7 ± 8.37 pg m^{-3}. Homo-yessotoxin represented 36.0% ± 10.3% of the total toxin content.

Meteorological and oceanographic data obtained from the SCCOOS automated shore station program (https://sccoos.org/autoss/#Data) were compared to the aerosolized YTX concentration (Table S2). A significant, positive correlation was found between the YTX concentration in the collected aerosols (Table S2) and both westerly winds (259–281 degree direction, p < 0.01; data not shown) and higher water level (p < 0.05; data not shown). By contrast, the total aerosolized YTX concentration did not correlate (p > 0.05) with either wind speed, wind gust, cell abundance *Lingulodinium polyedra,* or the YTX concentration in seawater (particulate + dissolved).
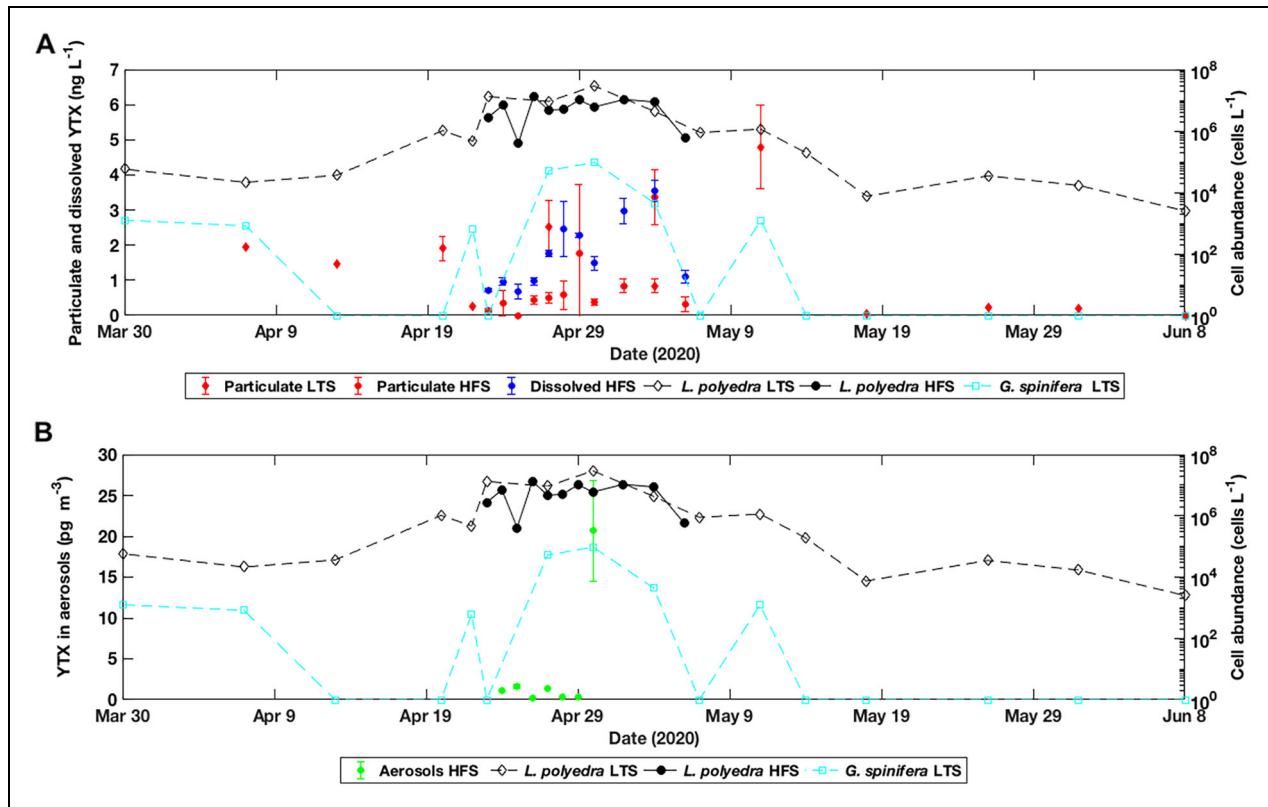
Figure 4. Concentrations of dissolved and particulate yessotoxin in seawater and aerosols during the 2020 red tide. Total yessotoxin (YTX) concentration with YTX producers, *Lingulodinium polyedra* (black lines) and *Gonyaulax spinifera* (cyan line), measured during the course of the bloom. (A) Total particulate (red) and dissolved (blue) YTX concentrations, with error bars (n = 3 and n = 2, respectively). The total dissolved YTX content increased throughout the bloom with a short decrease on April 30, 2020, and was higher than the total particulate YTX content most of the time. High-frequency sampling is shown as a continuous line with black circles; long-term sampling, as a dashed line with open diamonds. (B) Total YTX in aerosols (green) with error bars (n = 2), sampled April 24–30, remained stable throughout the bloom with a short increase on April 30. Cell abundance plotted on log scale to accommodate variability over the course of the bloom.

4. Discussion

4.1. Eukaryotic community

The establishment of the dense bloom of *Lingulodinium polyedra* in 2020 was concurrent with a sharp decrease in several other planktonic taxa (other dinoflagellates species, diatoms, and nanophytoplankton species). Initially, the bloom formed patches of high cell concentrations (Kahru et al., 2021) that rapidly became more widespread around April 26, most likely resulting from an aggregation of cells as often occurs at the sea surface in coastal upwelling systems (Ryan et al., 2008; Lai and Yin, 2014). High cell densities were maintained for a week, with at least two generations of cells stemming from either advection from offshore or cell reproduction, before they started to collapse on May 6. Abundances of *L. polyedra* were also recently shown to be shaped by the abundance of grazers, in particular ciliates (Kenitz et al., 2023). Species from the order Tintinnida were the most represented at the time, while the known ciliate predator *Favella ehrenbergii* (Stoecker et al., 1981) was not detected. Other known predators of *L. polyedra* include copepods of the Calanoida order (Prevett et al., 2019) and dinoflagellates such as *Fragilidium* spp. (Jeong et al., 1999), *Noctiluca scintillans*

(Busch et al., 2019), *Polykrikos* spp. (Jeong et al., 2001), and *Protoperidinium* spp. (Jeong and Latz, 1994). Even though the molecular data indicate an increase in the relative abundance of copepods of the Calanoida order towards the end of the bloom, the relative abundance of other protistan predators (*N. scintillans*, *Polykrikos* spp., and *Fragilidium* spp., ciliates) was higher at that time. Although known for infecting the dinoflagellate *Ceratium furca* (Lizárraga and Beltrones, 2003), the sharp increase of the relative abundance of the parasite *Amoebophrya* spp. could have also contributed to the demise of the bloom considering its role in terminating other red tides in California (Mazzillo et al., 2011).

4.2. Toxin pattern

The Californian strain of *Lingulodinium polyedra* is known to be a low YTX producer (Armstrong and Kudela, 2006; Howard et al., 2008), and the 2020 bloom was consistent with a total cellular YTX content ranging between 0 and 90.7 fg cell^{-1}. Elsewhere, the production of YTX by *L. polyedra* has been either similar (UK; Stobo et al., 2003) or higher (Italy and Spain; Draisci et al., 1998; Paz et al., 2004). However, the extreme cell concentration

achieved at the height of the bloom highlights the potential for HAB formation even at low per-cell toxin concentrations. Also, the detection of two unidentified ions, both showing *m/z* values and diagnostic fragments very close to the YTX and h-YTX (Figure S1) but eluting at different retention times, suggests the presence of isomeric forms of YTX analogs in the Californian strain. To be noted, the standard provided by the Cifga® company was isolated from a culture of *Protoceratium reticulatum*. In addition, most studies investigating YTX analogs (Ciminiello et al., 2003; Schirone et al., 2018) use low resolution mass spectrometry, leading to variable *m/z* values for YTX (1141.5 or 1141.6) and h-YTX (1155.5 or 1155.6), as well as for their diagnostic fragments. The use of high resolution mass spectrometry in this study indicates that both standard and isomeric forms of YTX may co-exist in the Californian strain. These putative isomers urgently need to be thoroughly identified, as they are detected at higher concentrations than the YTX and h-YTX (up to 416 fg cell^{-1}; Table S2).

Most planktonic dinoflagellate blooms exhibit a maximal particulate toxin concentration at the end of their exponential or stationary phases of growth (Anderson et al., 1990; Tester et al., 2008). Yet, during the 2020 *Lingulodinium polyedra* bloom event, some of the highest concentrations of particulate YTX coincided with the bloom initiation and demise, when the abundance of *L. polyedra* was relatively low. Several factors may have led to this pattern.

When examining the growth and cellular YTX content of three Swedish *L. polyedra* strains over time, Peter et al. (2018) found a reduced YTX production for faster-growing, long-lasting strains. The energy allocated to growth may interfere with the production of YTX in *L. polyedra*, resulting in low YTX production throughout the exponential phase of growth. Given the unprecedented cell abundances (over 29 million cells per liter), reached within only a few days and lasting for 2 weeks, the Californian strain can be considered a fast-growing, long-lasting strain (Juhl et al., 2000), which would therefore be consistent with low YTX production.

In several toxic dinoflagellates and diatoms, toxin production is modulated by copepod predation (Selander et al., 2015; Grebner et al., 2019) via the production of sulfated lipids called copepodamides (Selander et al., 2015). Although the effects of copepodamides on YTX production have not been measured for *L. polyedra*, the dinoflagellate reacts to copepodamides by producing a brighter flash of bioluminescence (Lindström et al., 2017) to deter the copepods (Prevett et al., 2019). Copepodamides are produced by at least two copepod species, *Calanus finmarchicus* and *Acartia tonsa* (Selander et al., 2015; Prevett et al., 2019), neither of which were known to be present during the bloom. The molecular data indicate that the copepod community was composed mainly of species belonging to the Calanoida family, such as *Paracalanus parvus* and other undefined species, whereas the Cyclopoida family, not known to produce copepodamides, dominated before the bloom. Given the absence of the known copepodamides (Selander et al., 2015; Selander et al., 2019) in the dissolved organic matter LC-HRMS full scan traces (data not shown) and a predation pressure applied mainly by other dinoflagellate species, the low YTX production during the bloom may reflect the minimal copepod predation or bottom-up drivers not measured.

Besides being a toxin producer, *Lingulodinium polyedra* is also renowned for its bioluminescence (Latz and Rohr, 1999). The peak of the bloom was associated with a particularly bright bioluminescence (Latzlab, 2020), providing further inputs to the debate on a shared enzymatic step for bioluminescence and toxin production (Cusick and Widder, 2020). In an *Alexandrium* species, bioluminescence-associated proteins are up-regulated during toxin production (Zhang et al., 2018), and several proteins similar to the luciferin binding protein are down-regulated in non-toxic mutants (Wang et al., 2012). Conversely, the high-bioluminescence observations concurrent with the period of low cellular YTX content suggests that there is no shared pathway for bioluminescence and YTX production for the southern Californian strain of *L. polyedra*. As bioluminescent reactions are energetically costly (Hastings, 1978) yet nevertheless highly selected by dinoflagellate species (Latz and Jeong, 1996), the energy allocated to bioluminescence during the 2020 bloom possibly may have affected YTX production negatively. However, identification of the genes and biosynthetic pathways responsible for the production of YTX would be necessary to decipher the relationship between bioluminescence and toxin production.

4.3. Transfer of YTX

The total dissolved toxin (YTX + h-YTX) content was measured during 2 weeks at the peak of the bloom and represented 51.3% to 100% of the total (particulate + dissolved) toxin content in seawater (0.87–6.89 ng L^{-1}). While particulate toxins have been found to account for the largest pool of total toxins in other dinoflagellate species (Tester et al., 2008; Pezzolesi et al., 2012; Ternon et al., 2022), similar findings to our results were seen in *L. polyedra* cultures (Paz et al., 2004). A continuous release of YTX might be characteristic of *L. polyedra* strains. In 2020, extracellular total YTX increased throughout the bloom, reaching its maximum level (3.54 ng L^{-1}) on May 4 at the peak of the bloom.

The presence of dissolved YTX and h-YTX in surface waters probably facilitated their transfer to sea spray aerosols (SSA), as has been shown for other organic molecules (Patterson et al., 2016; Rastelli et al., 2017). The aerosolization of h-YTX was recently demonstrated in a controlled system (Van Acker et al., 2021), with 0.78 ng m^{-3} detected in the SSA at a total seawater concentration of 33 µg L^{-1}. The maximum aerosol YTX concentration (YTX + h-YTX) was 0.021 ng m^{-3} during the 2020 bloom with a total seawater concentration of $1.85 \times 10^{-3} \pm 0.23$ µg L^{-1} (n = 3), suggesting higher enrichment factors of YTX analogs associated with natural blooms of *L. polyedra*. However, the aerosol YTX content did not correlate with the total YTX concentration in seawater (particulate + dissolved), in line with studies on brevetoxins and ovatoxins (Cheng et al., 2005; Ciminiello et al., 2014).

Environmental parameters such as wind direction and water level correlated well with aerosol YTX, indicating air–sea flux of toxins near the northern side of the Scripps Pier. Blooms of *Karenia brevis* in Florida yielded similar findings, with brevetoxins being detected and dispersed inland only in cases of onshore winds (Cheng et al., 2005; Kirkpatrick et al., 2010). The maximum aerosol YTX concentration of 29.0 pg m^{-3} was lower by a factor of 1000 than irritant aerosol concentrations for brevetoxin (57 ng m^{-3}; Fleming et al., 2009). However, if the putative isomeric forms of YTX analogs detected in this study were considered, the total YTX concentration would be estimated at 11.9 ng m^{-3} (Table S2), close to the irritant concentration of brevetoxin. In addition, a recent study showed that cell viability of pulmonary cell lines (A459 and BEAS-2B) is reduced by 50% at 1.31–3.87 µg L^{-1} of YTX (Van Acker et al., 2020); however, these concentrations were never reached during the bloom, whether the proposed isomeric forms were considered or not.

An informal survey conducted by the SCCOOS program reported significant respiratory syndromes during this 2020 bloom event. Additional investigation is necessary to determine whether YTX or other compounds were the possible cause of these symptoms. Indeed, similar symptoms are being reported increasingly by surfers during blooms of other dinoflagellate species, among which several are not known to be toxin producers (O'Halloran and Silver, 2021).

Not addressed by this study is whether YTX production by *Lingulodinium polyedra* contributed to the demise of fish and invertebrate populations in March 2020 (Skelton et al., n.d.), as was observed for red abalone in a deadly YTX event in northern California in 2011 (De Wit et al., 2014). The "forensic genomics" approach to examining the competing effects of YTX and hypoxia during that 2011 event inspired an investigation into the potential for YTX toxicity to wildlife in the 2020 bloom, and suggests a complicated chemical seascape during the historic 2020 "red tide" event in southern California that we are investigating further.

5. Conclusions

A *Lingulodinium polyedra* bloom of large size occurred in the Southern California Bight in the spring of 2020. Opportunistic sampling of the bloom at the onset of COVID-19 stay-at-home orders provided snapshots of bloom intensity and YTX content that have yielded new insights into YTX production by southern California *L. polyedra* strains and the transfer of that YTX to coastal aerosols where exposure to humans is greatest. While the *ad hoc* nature of the sampling under COVID stay-at-home orders did not allow for a full picture of bloom dynamics, it did yield the highest cell concentrations on record for *L. polyedra* in California and the first measurements of YTX in natural aerosols. The presence of YTX in aerosols motivates further investigation into YTX toxicity to better understand the threat it poses to animal and human health, particularly through airborne exposure.

Data accessibility statement

All molecular data are archived and available at the NCBI Sequence Read Archive under the BioProject accession number PRJNA923025.

Supplemental files

The supplemental files for this article can be found as follows:

Figure S1. Tables S1–S2. Docx

Competing interests

The authors declare no competing financial interest.

Author contributions

Conceptualization: ET, MLC, CRA, WHG.

Methodology: ET, MLC, RHL, WHG.

Formal analysis: ET, MLC, LC, RHL.

Investigation: ET, MLC.

Resources: MLC, CRA, AEA, KAP, WHG.

Data curation: ET, MLC, RHL.

Writing-original draft preparation: ET, MLC.

Writing-review and editing: ET, MLC, CRA, WHG, LC, RHL, KAP, AEA.

Funding acquisition: ET, MLC, CRA, KAP, AEA, WHG.

Approved the submitted version of the manuscript: All authors.

References

Alfonso, A, **Vieytes, MR**, **Botana, LM.** 2016. Yessotoxin, a promising therapeutic tool. *Marine Drugs* **14**(2): 30.

Allenlab. 2021. Protocol for processing 18Sv4 sequences in QIIME2. Available at https://github.com/

allenlab/QIIME2_18Sv4_ASV_protocol. Accessed November 30, 2023.

Anderson, DM, Kulis, DM, Sullivan, JJ, Hall, S, Lee, C. 1990. Dynamics and physiology of saxitoxin production by the dinoflagellates *Alexandrium* spp. *Marine Biology* **104**(3): 511–524. DOI: http://dx.doi.org/10.1007/BF01314358.

Armstrong, M, Kudela, R. 2006. Evaluation of California isolates of *Lingulodinium polyedrum* for the production of yessotoxin. *African Journal of Marine Science* **28**(2): 399–401. DOI: http://dx.doi.org/10.2989/18142320609504186.

Ault, AP, Moffet, RC, Baltrusaitis, J, Collins, DB, Ruppel, MJ, Cuadra-Rodriguez, LA, Zhao, D, Guasco, TL, Ebben, CJ, Geiger, FM, Bertram, TH. 2013. Size-dependent changes in sea spray aerosol composition and properties with different seawater conditions. *Environmental Science & Technology* **47**(11): 5603–5612. DOI: http://dx.doi.org/10.1021/es400416g.

Backer, LC, Kirkpatrick, B, Fleming, LE, Cheng, Y-S, Pierce, R, Bean, JA, Clark, R, Johnson, D, Wanner, A, Tamer, R, Zhou, Y, Baden, DG. 2005. Occupational exposure to aerosolized brevetoxins during Florida red tide events: Impacts on a healthy worker population. *Environmental Health Perspective* **113**(5): 644–649.

Balzano, S, Abs, E, Leterme, SC. 2015. Protist diversity along a salinity gradient in a coastal lagoon. *Aquatic Microbial Ecology* **74**(3): 263–277.

Bokulich, NA, Kaehler, BD, Rideout, JR, Dillon, M, Bolyen, E, Knight, R, Huttley, GA, Gregory Caporaso, J. 2018. Optimizing taxonomic classification of marker-gene amplicon sequences with QIIME 2's q2-feature-classifier plugin. *Microbiome* **6**(1): 1–17.

Bolyen, E, Rideout, JR, Dillon, MR, Bokulich, NA, Abnet, CC, Al-Ghalith, GA, Alexander, H, Alm, EJ, Arumugam, M, Asnicar, F. 2019. Reproducible, interactive, scalable and extensible microbiome data science using QIIME 2. *Nature Biotechnology* **37**(8): 852–857.

Busch, M, Caron, D, Moorthi, S. 2019. Growth and grazing control of the dinoflagellate *Lingulodinium polyedrum* in a natural plankton community. *Marine Ecology Progress Series* **611**: 45–58.

Callahan, BJ, McMurdie, PJ, Rosen, MJ, Han, AW, Johnson, AJA, Holmes, SP. 2016. DADA2: High-resolution sample inference from Illumina amplicon data. *Nature Methods* **13**(7): 581–583. DOI: http://dx.doi.org/10.1038/nmeth.3869.

Cheng, YS, Zhou, Y, Irvin, CM, Pierce, RH, Naar, J, Backer, LC, Fleming, LE, Kirkpatrick, B, Baden, DG. 2005. Characterization of marine aerosol for assessment of human exposure to brevetoxins. *Environmental Health Perspectives* **113**(5): 638–643.

Ciminiello, P, Dell'Aversano, C, Dello Iacovo, E, Fattorusso, E, Forino, M, Tartaglione, L, Benedettini, G, Onorari, M, Serena, F, Battocchi, C, Casabianca, S. 2014. First finding of *Ostreopsis* cf. *Ovata* toxins in marine aerosols. *Environmental Science & Technology*

48(6): 3532–3540. DOI: http://dx.doi.org/10.1021/es405617d.

Ciminiello, P, Dell'Aversano, C, Fattorusso, E, Forino, M, Magno, S, Guerrini, F, Pistocchi, R, Boni, L. 2003. Complex yessotoxins profile in *Protoceratium reticulatum* from north-western Adriatic sea revealed by LC–MS analysis. *Toxicon* **42**(1): 7–14. DOI: http://dx.doi.org/10.1016/S0041-0101(03)00094-1.

Cusick, KD, Widder, EA. 2020. Bioluminescence and toxicity as driving factors in harmful algal blooms: Ecological functions and genetic variability. *Harmful Algae* **98**: 101850. DOI: http://dx.doi.org/10.1016/j.hal.2020.101850.

De Wit, P, Rogers-Bennett, L, Kudela, RM, Palumbi, SR. 2014. Forensic genomics as a novel tool for identifying the causes of mass mortality events. *Nature Communications* **5**(1): 1–8.

Dierssen, HM, Kudela, RM, Ryan, JP, Zimmerman, RC. 2006. Red and black tides: Quantitative analysis of water-leaving radiance and perceived color for phytoplankton, colored dissolved organic matter, and suspended sediments. *Limnology and Oceanography* **51**(6): 2646–2659.

Dittmar, T, Koch, B, Hertkorn, N, Kattner, G. 2008. A simple and efficient method for the solid-phase extraction of dissolved organic matter (SPE-DOM) from seawater. *Limnology and Oceanography: Methods* **6**(6): 230–235. DOI: http://dx.doi.org/10.4319/lom.2008.6.230.

Draisci, R, Giannetti, L, Lucentini, L, Ferretti, E, Palleschi, L, Marchiafava, C. 1998. Direct identification of yessotoxin in shellfish by liquid chromatography coupled with mass spectrometry and tandem mass spectrometry. *Rapid Communications in Mass Spectrometry* **12**(19): 1291–1296. DOI: http://dx.doi.org/10.1002/(SICI)1097-0231(19981015)12:19<1291::AID-RCM314>3.0.CO;2-Y.

Fleming, LE, Bean, JA, Kirkpatrick, B, Chen, YS, Pierce, R, Naar, J, Nierenberg, K, Backer, LC, Wanner, A, Reich, A, Zhou, Y. 2009. Exposure and effect assessment of aerosolized red tide toxins (brevetoxins) and asthma. *Environmental Health Perspectives* **117**(7): 1095–1100. DOI: http://dx.doi.org/10.1289/ehp.0900673.

Grebner, W, Berglund, EC, Berggren, F, Eklund, J, Harðadóttir, S, Andersson, MX, Selander, E. 2019. Induction of defensive traits in marine plankton—New copepodamide structures. *Limnology and Oceanography* **64**(2): 820–831. DOI: http://dx.doi.org/10.1002/lno.11077.

Hallegraeff, G, Enevoldsen, H, Zingone, A. 2021. Global harmful algal bloom status reporting. *Harmful Algae* **102**: 101992. DOI: http://dx.doi.org/10.1016/j.hal.2021.101992.

Hallegraeff, GM. 2010. Ocean climate change, phytoplankton community responses, and harmful algal blooms: A formidable predictive challenge. *Journal of Phycology* **46**(2): 220–235. DOI: http://dx.doi.org/10.1111/j.1529-8817.2010.00815.x.

Hasle, R. 1978. The inverted microscope method, in Sournia, A ed., *Phytoplankton manual*. Paris, France: UNESCO: 88–96.

Hastings, J. 1978. [13] Bacterial bioluminescence: An overview. *Methods in Enzymology* **57**: 125–135.

Hatch, MB, Schellenberg, SA, Carter, ML. 2013. Ba/Ca variations in the modern intertidal bean clam *Donax gouldii*: An upwelling proxy? *Palaeogeography, Palaeoclimatology, Palaeoecology* **373**: 98–107.

Howard, MDA, Silver, M, Kudela, RM. 2008. Yessotoxin detected in mussel (*Mytilus californicus*) and phytoplankton samples from the U.S. west coast. *Harmful Algae* **7**(5): 646–652. DOI: http://dx.doi.org/10.1016/j.hal.2008.01.003.

Jeong, HJ, Kim, SK, Kim, JS, Kim, ST, Yoo, YD, Yoon, JY. 2001. Growth and grazing rates of the heterotrophic dinoflagellate *Polykrikos kofoidii* on red-tide and toxic dinoflagellates. *Journal of Eukaryotic Microbiology* **48**(3): 298–308. DOI: http://dx.doi.org/10.1111/j.1550-7408.2001.tb00318.x.

Jeong, HJ, Latz, M. 1994. Growth and grazing rates of the heterotrophic dinoflagellates *Protoperidinium* spp. on red tide dinoflagellates. *Marine Ecology Progress Series* **106**: 173.

Jeong, HJ, Shim, JH, Kim, JS, Park, JY, Lee, CW, Lee, Y. 1999. Feeding by the mixotrophic thecate dinoflagellate *Fragilidium* cf. *Mexicanum* on red-tide and toxic dinoflagellates. *Marine Ecology Progress Series* **176**: 263–277.

Juhl, AR, Velazquez, V, Latz, MI. 2000. Effect of growth conditions on flow-induced inhibition of population growth of a red-tide dinoflagellate. *Limnology and Oceanography* **45**: 905–915.

Kahru, M, Anderson, C, Barton, AD, Carter, ML, Catlett, D, Send, U, Sosik, HM, Weiss, EL, Mitchell, BG. 2021. Satellite detection of dinoflagellate blooms off California by UV reflectance ratios. *Elementa: Science of the Anthropocene* **9**(1): 00157. DOI: http://dx.doi.org/10.1525/elementa.2020.00157.

Kenitz, KM, Anderson, CR, Carter, ML, Eggleston, E, Seech, K, Shipe, R, Smith, J, Orenstein, EC, Franks, PJ, Jaffe, JS. 2023. Environmental and ecological drivers of harmful algal blooms revealed by automated underwater microscopy. *Limnology and Oceanography* **68**(3): 598–615.

Kirkpatrick, B, Pierce, R, Cheng, YS, Henry, MS, Blum, P, Osborn, S, Nierenberg, K, Pederson, BA, Fleming, LE, Reich, A. 2010. Inland transport of aerosolized Florida red tide toxins. *Harmful Algae* **9**(2): 186–189.

Lai, Z, Yin, K. 2014. Physical–biological coupling induced aggregation mechanism for the formation of high biomass red tides in low nutrient waters. *Harmful Algae* **31**: 66–75. DOI: http://dx.doi.org/10.1016/j.hal.2013.09.011.

Latz, M, Rohr, J. 1999. Luminescent response of the red tide dinoflagellate *Lingulodinium polyedrum* to laminar and turbulent flow. *Limnology and Oceanography* **44**(6): 1423–1435.

Latz, MI, Jeong, HJ. 1996. Effect of red tide dinoflagellate diet and cannibalism on the bioluminescence of the heterotrophic dinoflagellates *Protoperidinium* spp. *Marine Ecology Progress Series* **132**: 275–285.

Latzlab. 2020. It's a bioluminescent red tide! Images available at https://latzlab.ucsd.edu/2020/04/29/its-a-bioluminescent-red-tide/. Accessed November 30, 2023.

Lewis, ER, Schwartz, SE. 2004. *Sea salt aerosol production: Mechanisms, methods, measurements, and models*. Washington, DC: American Geophysical Union.

Lindström, J, Grebner, W, Rigby, K, Selander, E. 2017. Effects of predator lipids on dinoflagellate defence mechanisms—Increased bioluminescence capacity. *Scientific Reports* **7**(1): 13104. DOI: http://dx.doi.org/10.1038/s41598-017-13293-4.

Lizárraga, IG, Beltrones, DAS. 2003. Infection of *Ceratium furca* by the parasitic dinoflagellate *Amoebophyra ceratii* (Amoebophrydae) in the Mexican Pacific. *Acta Botanica Mexicana* **65**: 1–9.

Malfatti, F, Lee, C, Tinta, T, Pendergraft, MA, Celussi, M, Zhou, Y, Sultana, CM, Rotter, A, Axson, JL, Collins, DB, Santander, MV. 2019. Detection of active microbial enzymes in nascent sea spray aerosol: Implications for atmospheric chemistry and climate. *Environmental Science & Technology Letters* **6**(3): 171–177. DOI: http://dx.doi.org/10.1021/acs.estlett.8b00699.

Martin, M. 2011. Cutadapt removes adapter sequences from high-throughput sequencing reads. *EMBnet.journal* **17**(1): 10–12. DOI: http://dx.doi.org/10.14806/ej.17.1.200.

Mazzillo, FF, Ryan, JP, Silver, MW. 2011. Parasitism as a biological control agent of dinoflagellate blooms in the California current system. *Harmful Algae* **10**(6): 763–773.

McAlice, BJ. 1971. Phytoplankton sampling with the Sedgwick-Rafter cell. *Limnology and Oceanography* **16**(1): 19–28. DOI: http://dx.doi.org/10.4319/lo.1971.16.1.0019.

Medina-Pérez, NI, Dall'Osto, M, Decesari, S, Paglione, M, Moyano, E, Berdalet, E. 2021. Aerosol toxins emitted by harmful algal blooms susceptible to complex air–sea interactions. *Environmental Science & Technology* **55**(1): 468–477. DOI: http://dx.doi.org/10.1021/acs.est.0c05795.

NOAA ERDDAP. 2023. CalHABMAP—HABs Scripps Pier data. Available at https://erddap.sccoos.org/erddap/tabledap/HABs-ScrippsPier.html. Accessed November 30, 2023.

O'Halloran, C, Silver, M. 2021. Health risks and benefits among surfers after exposure to seawater in Monterey Bay, Santa Cruz County, California, United States. *Frontiers in Marine Science* **8**: 714831.

Patterson, JP, Collins, DB, Michaud, JM, Axson, JL, Sultana, CM, Moser, T, Dommer, AC, Conner, J, Grassian, VH, Stokes, MD, Deane, GB. 2016. Sea spray aerosol structure and composition using cryogenic transmission electron microscopy. *ACS Central*

Science **2**(1): 40–47. DOI: http://dx.doi.org/10.1021/acscentsci.5b00344.

Paz, B, Riobó, P, Luisa Fernández, M, Fraga, S, Franco, JM. 2004. Production and release of yessotoxins by the dinoflagellates *Protoceratium reticulatum* and *Lingulodinium polyedrum* in culture. *Toxicon* **44**(3): 251–258. DOI: http://dx.doi.org/10.1016/j.toxicon.2004.05.021.

Peter, C, Krock, B, Cembella, A. 2018. Effects of salinity variation on growth and yessotoxin composition in the marine dinoflagellate *Lingulodinium polyedra* from a Skagerrak fjord system (western Sweden). *Harmful Algae* **78**: 9–17. DOI: http://dx.doi.org/10.1016/j.hal.2018.07.001.

Pezzolesi, L, Guerrini, F, Ciminiello, P, Dell'Aversano, C, Dello Iacovo, E, Fattorusso, E, Forino, M, Tartaglione, L, Pistocchi, R. 2012. Influence of temperature and salinity on *Ostreopsis* cf. *Ovata* growth and evaluation of toxin content through HR LC-MS and biological assays. *Water Research* **46**(1): 82–92. DOI: http://dx.doi.org/10.1016/j.watres.2011.10.029.

Prevett, A, Lindström, J, Xu, J, Karlson, B, Selander, E. 2019. Grazer-induced bioluminescence gives dinoflagellates a competitive edge. *Current Biology* **29**(12): R564–R565. DOI: http://dx.doi.org/10.1016/j.cub.2019.05.019.

Rabines, A, Lampe, R, Allen, AE. 2020. Sterivex DNA extraction V.2. DOI: http://dx.doi.org/10.17504/protocols.io.bc2hiyb6.

Rastelli, E, Corinaldesi, C, Dell'Anno, A, Lo Martire, M, Greco, S, Cristina Facchini, M, Rinaldi, M, O'Dowd, C, Ceburnis, D, Danovaro, R. 2017. Transfer of labile organic matter and microbes from the ocean surface to the marine aerosol: An experimental approach. *Scientific Reports* **7**(1): 11475. DOI: http://dx.doi.org/10.1038/s41598-017-10563-z.

Rhodes, L, McNabb, P, de Salas, M, Briggs, L, Beuzenberg, V, Gladstone, M. 2006. Yessotoxin production by *Gonyaulax spinifera*. *Harmful Algae* **5**(2): 148–155. DOI: http://dx.doi.org/10.1016/j.hal.2005.06.008.

Robeson, MS, O'Rourke, DR, Kaehler, BD, Ziemski, M, Dillon, MR, Foster, JT, Bokulich, NA. 2021. RESCRIPt: Reproducible sequence taxonomy reference database management. *PLoS Computational Biology* **17**(11): e1009581.

Ryan, JP, Gower, JF, King, SA, Bissett, WP, Fischer, AM, Kudela, RM, Kolber, Z, Mazzillo, F, Rienecker, EV, Chavez, FP. 2008. A coastal ocean extreme bloom incubator. *Geophysical Research Letters* **35**(12). DOI: http://dx.doi.org/10.1029/2008GL034081.

Sala-Pérez, M, Alpermann, TJ, Krock, B, Tillmann, U. 2016. Growth and bioactive secondary metabolites of arctic *Protoceratium reticulatum* (Dinophyceae). *Harmful Algae* **55**: 85–96. DOI: http://dx.doi.org/10.1016/j.hal.2016.02.004.

Satake, M, MacKenzie, L, Yasumoto, T. 1997. Identification of *Protoceratium reticulatum* as the biogenetic origin of yessotoxin. *Natural Toxins* **5**(4): 164–167. DOI: http://dx.doi.org/10.1002/19970504NT7.

Schirone, M, Berti, M, Visciano, P, Chiumiento, F, Migliorati, G, Tofalo, R, Suzzi, G, Di Giacinto, F, Ferri, N. 2018. Determination of lipophilic marine biotoxins in mussels harvested from the Adriatic sea by LC-MS/MS. *Frontiers in Microbiology* **9**: 152.

Selander, E, Berglund, EC, Engström, P, Berggren, F, Eklund, J, Harðardóttir, S, Lundholm, N, Grebner, W, Andersson, MX. 2019. Copepods drive large-scale trait-mediated effects in marine plankton. *Science Advances* **5**(2): eaat5096. DOI: http://dx.doi.org/10.1126/sciadv.aat5096.

Selander, E, Kubanek, J, Hamberg, M, Andersson, MX, Cervin, G, Pavia, H. 2015. Predator lipids induce paralytic shellfish toxins in bloom-forming algae. *Proceedings of the National Academy of Sciences* **112**(20): 6395–6400. DOI: http://dx.doi.org/10.1073/pnas.1420154112.

Skelton, ZR, McCormick, LR, Kwan, GT, Lonthair, J, Neira, C, Clements, SM, Martz, TR, Bresnahan, PJ, Send, U, Giddings, SN, Sevadjian, JC, Jaeger, S, Feit, A, Frable, BW, Zerofski, PJ, Torres, M, Crooks, JA, McCullough, J, Carter, ML, Ternon, E, Miller, LP, Kalbach, GM, Wheeler, DC, Parnell, PE, Swiney, KM, Seibert, G, Minich, JJ, Hyde, JR, Hastings, PA, Smith, JE, Komoroske, LM, Tresguerres, M, Levin, LA, Wegner, NC. n.d. Organismal responses to deteriorating water quality during the historic 2020 red tide off Southern California. *Elementa: Science of the Anthropocene*, submitted, under review.

Stobo, LA, Lewis, J, Quilliam, MA, Hardstaff, WR, Gallacher, S, Webster, L, Smith, E, McKenzie, M. 2003. Detection of yessotoxin in UK and Canadian isolates of phytoplankton and optimization and validation of LC-MS methods. *Canadian Technical Report of Fisheries and Aquatic Sciences* **2498**: 8–14.

Stoecker, D, Guillard, RRL, Kavee, RM. 1981. Selective predation by *Favella ehrenbergii* (Tintinnia) on and among dinoflagellates. *The Biological Bulletin* **160**(1): 136–145.

Ternon, E, Pavaux, A-S, Peltekis, A, Gemin, M-P, Jauzein, C, Bailleul, B, Lemée, R, Thomas, OP. 2022. Assessment of the allelochemical activity of Ostreopsis cf. *Ovata* and the ovatoxins towards competitive benthic microalgae. *Aquatic Ecology* **56**(2): 475–491.

Tester, PA, Shea, D, Kibler, SR, Varnam, SM, Black, MD, Litaker, WR. 2008. Relationships among water column toxins, cell abundance and chlorophyll concentrations during *Karenia brevis* blooms. *Continental Shelf Research* **28**(1): 59–72. DOI: http://dx.doi.org/10.1016/j.csr.2007.04.007.

Van Acker, E, De Rijcke, M, Asselman, J, Beck, IM, Huysman, S, Vanhaecke, L, De Schamphelaere, KAC, Janssen, C. 2020. Aerosolizable marine phycotoxins and human health effects: *In vitro* support for the biogenics hypothesis. *Marine Drugs* **18**(1): 46.

Van Acker, E, **Huysman, S**, **De Rijcke, M**, **Asselman, J**, **De Schamphelaere, KAC**, **Vanhaecke, L**, **Janssen, CR.** 2021. Phycotoxin-enriched sea spray aerosols: Methods, mechanisms, and human exposure. *Environmental Science & Technology* **55**(9): 6184–6196. DOI: http://dx.doi.org/10.1021/acs.est.1c00995.

Van Eijk, AMJ, **Kusmierczyk-Michulec, JT**, **Francius, MJ**, **Tedeschi, G**, **Piazzola, J**, **Merritt, DL**, **Fontana, JD.** 2011. Sea-spray aerosol particles generated in the surf zone. *Journal of Geophysical Research: Atmospheres* **116**(D19). DOI: http://dx.doi.org/10.1029/2011JD015602.

Wang, D-Z, **Li, C**, **Zhang, Y**, **Wang, Y-Y**, **He, Z-P**, **Lin, L**, **Hong, H-S.** 2012. Quantitative proteomic analysis of differentially expressed proteins in the toxicity-lost mutant of *Alexandrium catenella* (Dinophyceae) in the exponential phase. *Journal of Proteomics* **75**(18): 5564–5577. DOI: http://dx.doi.org/10.1016/j.jprot.2012.08.001.

Wilson, JM, **Erazo, N**, **Connors, E**, **Chamberlain, EJ**, **Clements, SM**, **Carter, ML**, **Smith, JE**, **Bowman, JS.** 2022. Substantial microbial community shifts in response to an exceptional harmful algal bloom in coastal Southern California. *Elementa: Science of the Anthropocene* **10**(1): 00088. DOI: http://dx.doi.org/10.1525/elementa.2021.00088.

Zhang, S-F, **Zhang, Y**, **Lin, L**, **Wang, D-Z**. 2018. iTRAQ-based quantitative proteomic analysis of a toxigenic dinoflagellate *Alexandrium catenella* at different stages of toxin biosynthesis during the cell cycle. *Marine Drugs* **16**(12): 491.

ELEMENTA
Science of the Anthropocene

Elem Sci Anth is a peer-reviewed open access journal published by University of California Press.

OPEN ACCESS